Journal of Physics: Conference Series

Thermo-physical properties of paraffin wax with iron oxide nanoparticles as phase change material for heat storage applications

Thermo-physical properties of paraffin wax with iron oxide nanoparticles as phase change material for heat storage applications

Meriem JEBALI [1], Gianpiero COLANGELO [1], Laia HAURIE [2], Imene BEKRI-ABBES [3], Ana Maria LACASTA [2]

[1] Department of Engineering for Innovation - University of Salento, Lecce, Italy
[2] Department of Building Construction and Architecture - Polytechnic University of Catalonia (UPC), Barcelona, Spain
[3] National Center for Researches in Materials Sciences, Technopole of Borj Cedria, Soliman, Tunisia

Corresponding author, email: gianpiero.colangelo@unisalento.it

Abstract. Phase change materials (PCMs) are growing in importance in many thermal applications as heat storage or to smooth the energy peak demand in many technological fields in industrial as well as in civil applications. Conductive nanoparticles can be added to phase change material to improve their thermo-physical properties. In this work, Iron oxide nanoparticles (IOx-NPs) were synthesized using a simple and green synthesis method, free of toxic and harmful solvents, using the extract of a plant as a reducer and stabilizer at two different temperatures of calcination 500°C and 750°C. The metallic oxide was used as an additive with 2% wt. compositions to paraffin wax to prepare a nanocomposite. The variation in thermal properties of paraffin wax in the composite was experimentally investigated. The biosynthesized IOx-NPs were characterized by X-ray diffraction (XRD), Fourier Transform Infrared Spectroscopy (FTIR) and Scanning Electron Microscope (SEM) and Thermal Gravimetric Analysis (TGA) techniques. The thermal properties of the synthesized nanocomposites were characterized by a thermal conductivity analyzer and differential scanning calorimetry (DSC). The FTIR spectra showed a bond at 535 cm-1, which confirms the Fe-O vibration. The XRD powder analysis revealed the formation of the cubic phase of Fe_3O_4 with an average particle size of 11 nm at 500°C and the presence of the phase α-Fe_2O_3 with Fe_3O_4 at 750°C. Scanning Electron Microscopy (SEM) showed that the obtained oxide was made up of particles of nanoscale size. Experimental measurements showed that the presence of nanoparticles can improve the latent heat capacity by a maximum of 16.16 % and the thermal conductivity of the nanocomposites by a maximum of 16.99%.

Keywords: c, PCM, thermal conductivity, composites

1. Introduction

Among the various energy storage techniques based on renewable resources, thermal energy storage (TES) plays a major role to balance the demand and supply of energy by storing the thermal energy and releasing it when necessary [1]. Phase change material (PCM) is the most used form for latent thermal energy storage (LTES) due to its isothermal behavior during the heat storage/release process [2]. The applications of PCM depend generally on the melting temperature (Tm). When Tm is in the range of 0-15°C, the PCM is used for air conditioning systems. Although, when Tm is above 85°C, the PCM is mainly used for industrial, solar energy and aerospace application. The PCM that melts between 15°C

and 85°C could be used in heat sinks for high power electronic cooling and building applications [1]. This type of PCMs received more attention because of the high energy consumption in its application sectors [3]. Over the past decades, paraffin waxes (Tm around 55°C) have been considered to be one of the most important forms of PCM used for latent heat thermal energy storage systems (LHTESs) [2,4]. It is becoming progressively attractive because of its good stability, non-toxicity, high energy storage density, non-supercooling, and an appropriate phase change temperature [5]. However, due to its low thermal conductivity TC (~ 0.2 W/mK), many methods and studies have been reported in literature to improve the thermal performance of LHTESs and extend their application range [2, 6–9]. To solve this limitation, a determined amount of nanoparticles has been added to the PCM during the melting process. Various experimental factors and conditions have been investigated regarding the influence of the presence of nanoparticles in the PCM on the thermal conductivity and the latent heat capacity of the composites. So far, a variety of nanoparticle materials dispersed in PCM has been studied, including alumina [7,8] , copper oxide [3], titania [7], ferric oxide [10] , silica [7,8], zinc oxide [7,10,11] and carbon-based materials [2,9]. Iron oxide nanoparticles (IOx-NPs) and their nanocomposites have been chosen in this study because of their thermal behavior.

The objective of this work is:

i. To prepare iron oxide through a green, simple and low-cost method using an extract plant at two different temperatures of calcination.
ii. To investigate the physicochemical properties of the elaborated nanoparticles.
iii. To analyze the thermal properties of paraffin wax by adding 2% (by weight) of iron oxides and to observe the enhancement of TC and LHC of the nanocomposites in the presence of the biosynthesized IOx-NPs.

The structure and the morphology of the IOx-NPs were characterized using X-ray diffraction (XRD), Fourier transform infrared spectroscopy (FTIR), Scanning electron microscope (SEM), and Thermogravimetric analysis (TGA). The thermal properties of the prepared nanocomposites were characterized by a thermal conductivity analyzer and differential scanning calorimetry (DSC).

2. Experimental characterizations

2.1. Materials

The paraffin was obtained from a local industry. The iron precursor $Fe(NO_3)_3 \cdot 9H_2O$ extra pure 99% was purchased from SRLchem and used as received. Fresh lemon fruits purchased from a local market. Distilled water was used in all experimental work.

2.2. Preparation of Iron oxide nanoparticles

The required amount of Iron (III) nitrate nanohydrate $Fe(NO_3)_3 \cdot 9H_2O$ was first dissolved in distilled water. The solution was magnetically stirred at room temperature for 30 minutes before adding the lemon juice extract as a green fuel in stoichiometric quantities. Then the solution was vigorously stirred at 80°C until it began to burn and then released a large amount of heat. The combustion reaction duration was 20 minutes, resulting in a dark brown precipitate indicating the iron oxide nanoparticles formation. To remove all organic impurities and any attached molecule of water, the dried precipitate was placed in a silica crucible and subjected to calcination in a muffle furnace at 500°C for 2h (IOx-500). The same procedure was repeated by modifying the calcination temperature to be at 750°C for 2h (IOx-750).

2.3. Preparation of PCM nanocomposites

To prepare the PCM composites, paraffin wax (PW) was first melted at 70°C. IOx-NPs were added to the melted PW to form mixtures that have been thoroughly stirred at 70°C by a magnetic stirrer/hot plate for 1h. Then the mixtures were subjected to an intensive ultrasound for 30 min using a sonicator (Model:

VCX 130; 130 W; 20 kHz) to prepare nanocomposites well dispersed within the PW. The nanocomposite was then poured into a cast and allowed to solidify. The prepared nanocomposites were prepared with 2% by weight of IOx-NPs, with a reference sample of pure paraffin wax.

2.4. Characterization techniques

X-ray diffraction (XRD) patterns of IOx-NPs, PW and nanocomposites were recorded by using a powder X-ray diffractometer Rigaku using monochromatic CuKα radiation (λ = 1.54 Å) with a counting time of 0.002 ° / s (2θ). The obtained diffractogram was processed with the X'pert High Score Plus software. The morphology and the microstructure of IOx-NPs were observed by Scanning Electron Microscopy (SEM) (20 kV, magnification 7 000 X and 10 500 X). Fourier transform infrared (FT-IR) spectra were measured by TwoTM from Perkin Elmer (400 - 4000 cm^{-1} working range) supported by Dynascan™ interferometer and OpticsGuardTM technology with attenuated total reflectance (ATR). This equipment was optimized by a wavelength range between 4000 cm^{-1} and 400 cm^{-1} and its standard spectral resolution was 0.5 cm^{-1}. Thermogravimetric analysis (TGA) was carried out using a thermal gravimetric analysis instrument with a heating rate of 10°C/min in Nitrogen. The differential scanning calorimetry (DSC) analysis was studied at the scan rate of 10°C/min over the range of 10-90°C.

2.5. Error analysis

Error estimation of used instruments are provided. The details of microstructural analysis, DSC analysis, thermal conductivity measurement and temperature measurement are shown in Table 1.

Table 1. Accuracy of the used instruments.

Instrument / characterization method	Accuracy
Rigaku XRD diffractometer	± 0.00004˚
DSC analysis	± 0.1 °C Temperature
	± 2% Latent heat
Thermal properties analyzer (Quickline-30)	± 1% Thermal conductivity

3. Results and discussions

3.1. XRD analysis

The X-ray diffraction (XRD) analysis was used to determine the crystallographic parameters of the elaborated sample. XRD diffractograms for iron oxide calcined at different temperatures of 500°C (IOx-500) and 750°C (IOx-750), PW and nanocomposites are shown in figure 1 (a-e). The diffraction peaks of IOx-500 in figure 1(a) were observed at positions 2θ = 18.19°; 30.10 °; 35.32°; 37.02°; 42.99°; 53.51°; 57.07°; 62.63°; 71.20° and 74.18° and assigned in terms of the Miller indices (hkl) correspond respectively to the diffraction planes (111), (220), (311), (222), (400), (422), (511), (440), (620) and (422). No additional peaks from impurities were detected, which confirms the high purity of the Fe_3O_4 nanoparticles calcined at 500°C without the presence of other crystalline phases. The magnetite Fe_3O_4 crystallizes in a cubic structure as per the JCPDS N° 01-088-0315 and exhibits the F d-3m space group as the XRD pattern shows. The bioactive compounds that are present in the lemon fruit extract such as flavonoids, polyphenols and tannins are responsible for the formation of iron oxide nanoparticles [12]. However, the diffractogram of IOx-750 in figure 1(b) shows additional peaks of the α-Fe_2O_3 phase. These results confirm the influence of the calcination temperature on the powder's crystallinity. The

average size of the samples IOx-500 and IOx-750 are about 11 and 29 nm. The average sizes of the particles were calculated by using the Scherrer equation [13] which is shown below in equation (1):

$$D = \frac{K\lambda}{\beta \cos\theta} \quad (1)$$

Where D is the average crystallite size, K is the Scherrer constant (0.9), λ is the wavelength of the X-ray beam used, CuKα (λ = 1.54 Å), β is the full width at half maximum intensity of the peak (FWHM) and θ is the Bragg's angle.

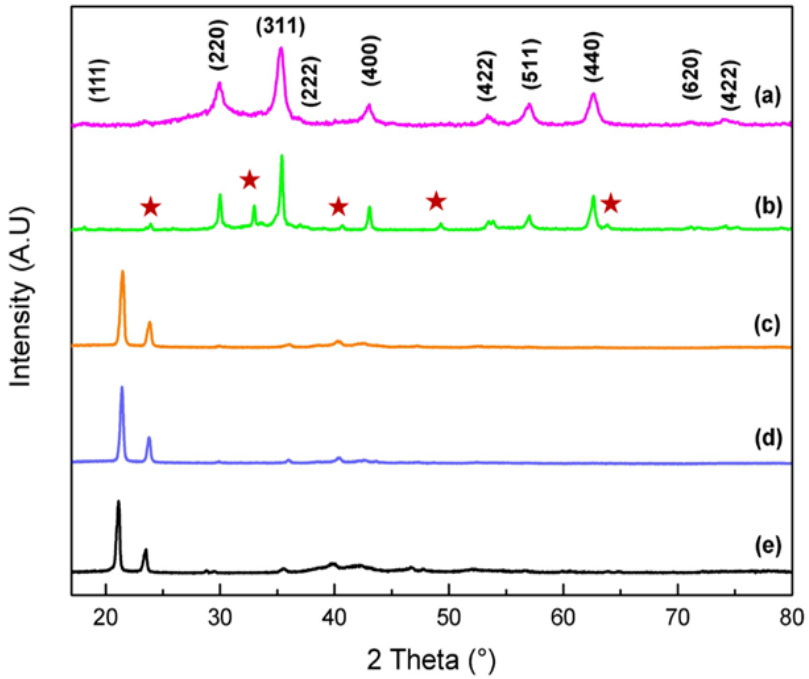

Figure 1:XRD pattern of (a) IOx-500, (b) IOx-750 (the red stars referred to as the characteristic peaks of the hematite α-Fe2O3), (c) PW/IOx-500, (d) PW/IOx-750 and (e) PW.

The diffractogram of the PCM in figure 1(e) confirms that all the diffraction peaks were belonging to paraffin wax (JCPDS N° 00-003-0254). The XRD patterns of PW/IOx-500 and PW/IOx-750 in figure 1 (c,d) indicated the existence of the same sets of diffraction peaks observed for the pure paraffin wax. This result could be explained as the presence of the iron oxide nanoparticles does not change the crystalline structure of the PCM [10]. The XRD results show that during the preparation of the nanocomposites there is no chemical interaction between the PCM and the metal oxide to maintain the purity of their different crystal lattice [11].

3.2. SEM analysis

The morphology and the size distribution of the samples IOx-500 and IOx-750 were investigated with SEM and reported in figure 2 (a,b) to identify if the existence of any changes in the iron oxide

nanoparticles while modifying the temperature of calcination from 500°C to 750°C. Figure 2 (a) shows the SEM image of the sample IOx-500 (Fe_3O_4) prepared by the green method. IOx-500-NPs have a spherical shape structure and some were agglomerated with an average distribution size of about 54 nm, which was consistent with other works [14–16]. However, in figure 2 (b), the morphology of the sample IOx-750 changed to a cubic shape with a size range of 100-700 nm. The inspection of SEM clearly shows that the annealing process forced the small particles to coalesce into larger particles with different shapes. It is interesting to note that the morphology of the IOx-500 sample changes from spherical particles to a cubic aspect by changing only the calcination temperature and that the size of the particles is changed when increasing the temperature. This suggests that the calcination temperature during the synthesis can effectively adjust the shape and size of the particles.

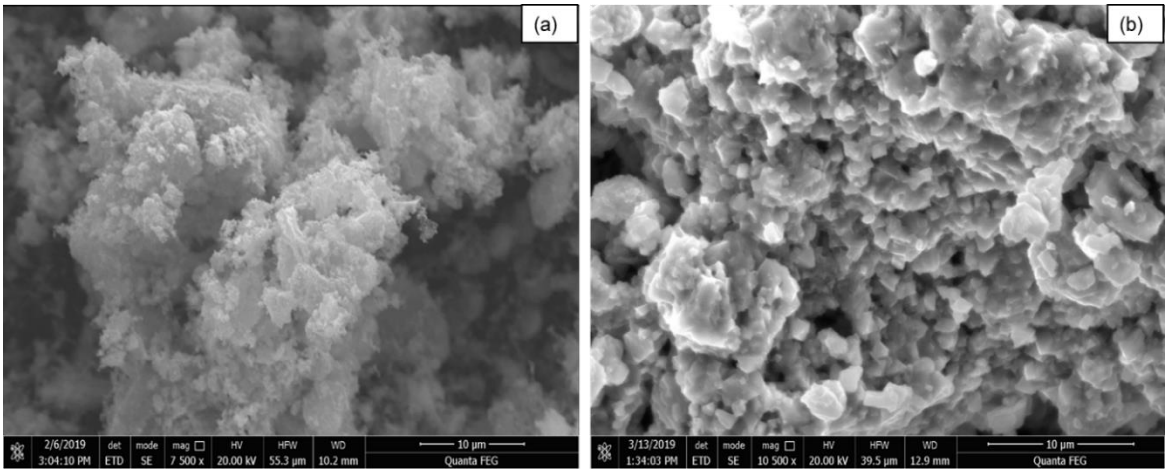

Figure 2:SEM micrographs of IOx-NPs (a) IOx-500 and (b) IOx-750.

3.3. FTIR Spectroscopy

The FTIR spectrum of the iron oxide nanoparticles, paraffin wax, and composites are shown in figure 3. The FTIR Spectrum of IOx-500 and IOx-750 in figure 3 (e,d) exhibited characteristic bands positioned at 3344, 1552, 1370, 1110, 1022 and 535 cm^{-1}. The absorption band at 3344 cm^{-1} was related to the O-H vibration of the phenolic compound acting as a reducing agent in the formation of iron oxide nanoparticles [17]. The band observed at 1552 cm^{-1} was attributed to the C=O stretching. The band at 1370 cm^{-1} was associated to C=C vibration of aromatic compound which revealed the functionalization of the prepared nanoparticles with organic compounds [18]. The bands at 1110 and 1022 cm^{-1} were attributed to the aromatic rings and their functional groups present in the organic compounds in the lemon extract [11]. The characteristic band observed at 535 cm^{-1} corresponding to the stretching vibration of Fe-O [17,18], confirmed the formation of iron oxides. In addition, the FTIR spectrum of the PW/IOx-500 and PW/IOx-750 composites and the pure paraffin wax have been demonstrated in figure 3 (a), (d) and (c), respectively. The absorption bands at 2959, 2916, 2847, 1463, 1378, 893 and 720 cm^{-1} are attributed to –C=H3 and C=H2 stretching, C=C symmetric stretching, =C-H bending, =C-H and =C-H2 vibration and –CH2, respectively [19].

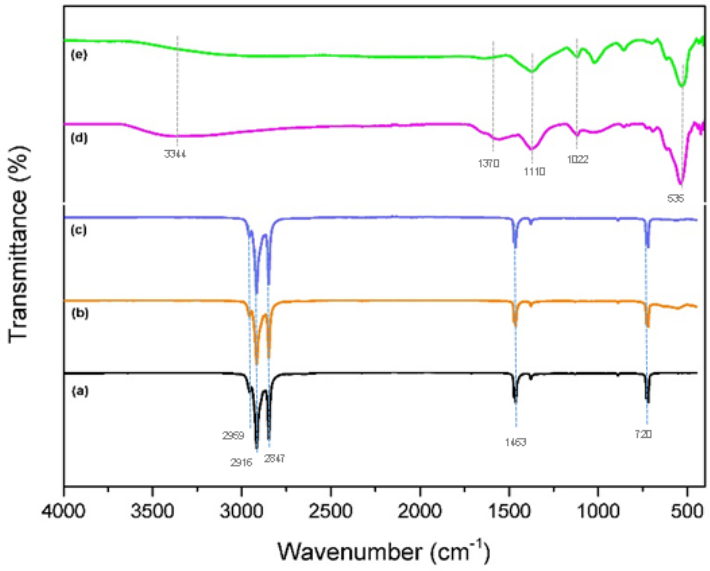

Figure 3:FTIR spectra of (a) PW, (b) PW/IOx-500, (c) PW/IOx-750, (d) IOx-500 and (e) IOx-750.

3.4. TGA analysis

In the TGA curve of Fe_3O_4 (IOx-500) in figure 4, the weight loss (~ 2.40%) below 117.7°C can be attributed to the release of water. The second weight-loss step (~ 1.63%) was seen at 117.7-188.3°C which endorsed the evaporation of moisture [20]. Around (4.18%) of weight-loss was carried out owing to decomposition of organic matter between 188.3 and 506°C. When the temperature increased, mass loss (~ 2%) from 506 to 859°C was mainly due to the phase transformation from maghemite (Fe_3O_4) to hematite (Fe_2O_3) [21].

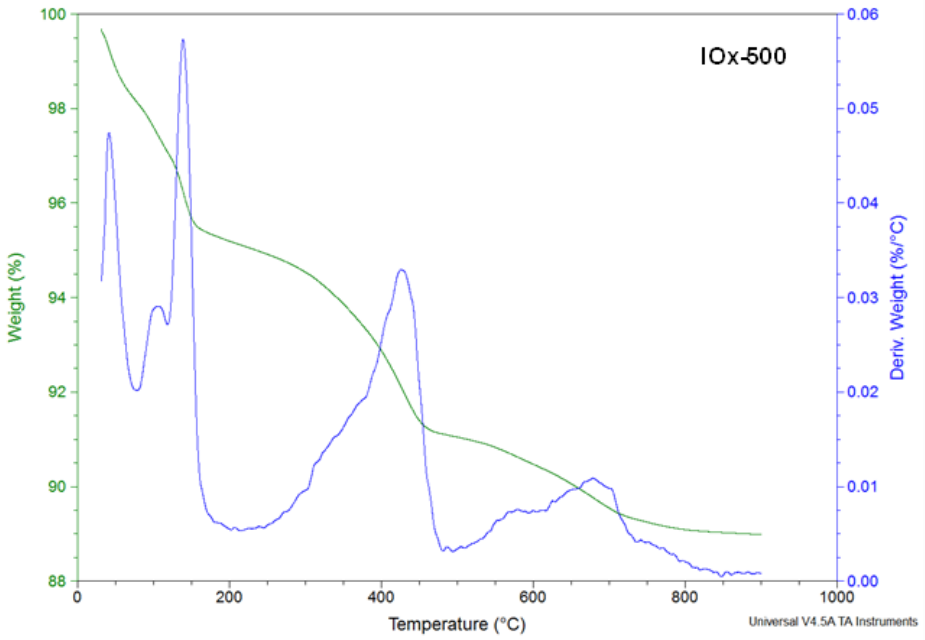

Figure 4: TGA/DTA curve of the sample IOx-500.

3.5. Thermal properties of nanocomposites

3.5.1. DSC analysis

The effect of nano-additives on the melting points, the freezing points, and the latent heats of the composites were analyzed by DSC. Figure 5 shows the solid-liquid phase change latent heat (LH) and the temperature of the pure paraffin wax (PW) and the iron oxide nanoparticles doped paraffin during the melting and cooling processing at the scan rate of 10°C/min over the range 10-90°C. From DSC curves, the energy under the endothermic and exothermic peaks of the pure paraffin was integrated given LH of 206.03 and 187.74 J/g for melting and cooling, respectively, which differed by 8.87%. According to Mikhaylov et al. [22], this difference could be attributed to some change in the heat capacity versus temperature dependency.

The melting enthalpies of PW/IOx-500 and PW/IOx-750 are 218.02 and 209.23 J/g, respectively. However, the cooling enthalpies are 218.08 and 216.09 J/g. The addition of 2% (by weight) of iron oxide nanoparticles increased the LH value by 5.82% and 1.55% during the melting process and by 16.16% and 15.10% during the crystallization process of the samples PW/IOx-500 and PW/IOx-750 respectively, compared to the pure paraffin. The increase of the LH of the nanocomposites could be attributed to the possible interaction between the paraffin wax and the iron oxide [23].
Furthermore, the peaks melting and cooling temperatures of pure paraffin are 66.35°C and 58.41°C. The peaks temperature during the melting process (T_m) of the composites PW/IOx-500 and PW/IOx-750 are 66.11°C and 65.62°C, respectively. Similarly, the peak temperature during the crystallization process (T_c) of the composites are 60.12°C and 60.47°C. As it can be seen, the addition of 2% (by weight) of IOx-NPs in paraffin reduced the T_m and increased the T_c. This demonstrated that adding of iron oxide nanoparticles reduced the supercooling of the PW by acting as nucleation agent [24]. All the results of the melting and cooling LHs and the peak temperatures are shown in table 2.

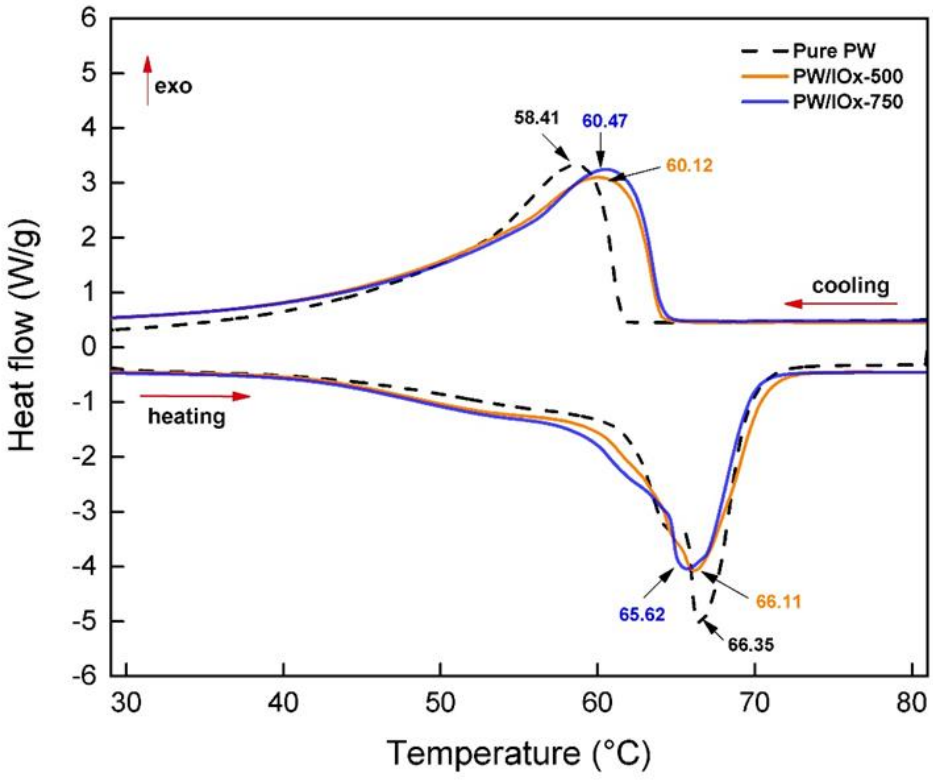

Figure 5:DSC thermograms of the pure PW and the composites

Table 2. Thermal Properties of pure PW and the nanocomposites PW/IOx-500 and PW/IOx-750.

Sample	Mass ratio of nanoparticles (%)	Melting process		Crystallization process	
		T_m (°C)	ΔH_m (J/g)	T_c (°C)	ΔH_c (J/g)
PW	0	66.35	206.03	58.41	187.74
PW/IOx-500	2	66.11	218.02	60.12	218.08
PW/IOx-750	2	65.62	209.23	60.47	216.09

3.5.2. Thermal conductivity measurement

The thermal conductivity (TC) of the PW and the nanocomposites was measured by a Quickline-30 thermal properties analyzer. The measurements were repeated five times for every sample at a fixed temperature and the average value was reported. The thermal conductivity of the pure paraffin wax is 0.259 W/mK. For the samples with 2% (by weight) PW/IOx-500 and PW/IOx-750, the thermal conductivity increased to 0.298 and 0.303 W/mK, respectively. Sahan et al. [25] reported that the dispersion of 10 wt% and 20 wt% of Fe_3O_4 in paraffin could enhance the TC by 48% and 60%, respectively. The thermal conductivity enhancement (TCE) of the samples PW/IOx-500 and PW/IOx-750 was calculated by the equation 2 shown below:

$$\mathrm{TCE} = \frac{K_{nanocomposites} - K_{PW}}{K_{PW}} \quad (2)$$

Where $\boldsymbol{K}_{\text{nanocomposites}}$ is the measured TC of the samples PW/IOx-500 and PW/IOx-750 and $\boldsymbol{K}_{\text{PW}}$ is the TC of the pure paraffin wax.

The TCE of PW/IOx-500 and PW/IOx-750 are 15.05% and 16.99%, respectively. This result indicates that the TCs of the nanocomposites are higher than the pure paraffin wax as shown in table 3. The improvement in the TCs principally assigned to the high TC of nanoparticles.

Table 3. Thermal conductivity measurements of PW, PW/IOx-500 and PW/IOx-750.

Samples	Mass ratio of nanoparticles (%)	Measured Thermal Conductivity at 25°C	TCE (%)
PW	0	0.259 W/m K	-
PW/IOx-500	2	0.298 W/m K	15.05 %
PW/IOx-750	2	0.303 W/m K	16.99 %

4. Conclusion

Iron oxide nanoparticles IOx-Nps were successfully prepared via a novel green synthesis using extract of lemon fruit at two different temperatures (500°C and 750°C) and it was confirmed by X-ray diffraction (XRD), Scanning electron microscope (SEM), Fourier transform infrared spectroscopy (FTIR) and Thermogravimetric analysis (TGA). The XRD results showed that the particle sizes were 11 nm and 29 nm for the samples IOx-500 and IOx-750 without any addition of surfactants. The SEM images showed that the size and the morphology of the nanoparticles have been changed when increasing the temperature during the annealing process. In this study, paraffin wax (PW) was used as a phase change material (PCM) and 2% by weight of the prepared IOx-NPs have been added to PW to form nanocomposites. The thermal properties of the nanocomposites have been investigated and compared to the pure PW. Experimental results revealed that the presence of the IOx-NPs increased the latent heat value by 5.82% and 1.55% during the melting process and by 16.16% and 15.10% during the crystallization process of the samples PW/IOx-500 and PW/IOx-750 respectively, compared to the pure PW. Besides these results, the thermal conductivity (TC) has been improved by 15.05% and 16.99% for the samples PW/IOx-500 and PW/IOx-750 compared to the pure PW. These results confirm that paraffin wax green iron oxide nanoparticles-based composites have a good thermal performance for heat storage applications.

Acknowledgments

This work was possible thanks to the technical support of Prof. Christian Demitri, Mr. Francesco Montagna and Mr. Donato Cannolletta of University of Salento.

6. References

[1] Faraji H and Benkaddour A 2020 Emerging applications of phase change materials : A concise review of recent advances

[2] Xia L, Zhang P and Wang R Z 2010 Preparation and thermal characterization of expanded graphite/paraffin composite phase change material *Carbon N. Y.* **48** 2538–48

[3] Chandrasekaran P, Cheralathan M, Kumaresan V and Velraj R 2014 Enhanced heat transfer characteristics of water based copper oxide nanofluid PCM (phase change material) in a spherical capsule during solidification for energy efficient cool thermal storage system *Energy* **72** 636–42

[4] Muhammad H, Arshad A, Jabbal M and Verdin P G 2018 International Journal of Heat and Mass Transfer Thermal management of electronics devices with PCMs filled pin-fin heat sinks : A comparison *Int. J. Heat Mass Transf.* **117** 1199–204

[5] Kousksou T, Jamil A, Rhafiki T El and Zeraouli Y 2010 Solar Energy Materials & Solar Cells Paraffin wax mixtures as phase change materials *Sol. Energy Mater. Sol. Cells* **94** 2158–65

[6] Farid M M, Khudhair A M, Ali S and Razack K 2004 A review on phase change energy storage : materials and applications **45** 1597–615

[7] Teng T P and Yu C C 2012 Characteristics of phase-change materials containing oxide nano-additives for thermal storage *Nanoscale Res. Lett.* **7**

[8] Chieruzzi M, Cerritelli G F, Miliozzi A and Kenny J M 2013 Effect of nanoparticles on heat capacity of nanofluids based on molten salts as PCM for thermal energy storage *Nanoscale Res. Lett.* **8** 1–9

[9] Xiao X and Zhang P 2013 Morphologies and thermal characterization of paraffin/carbon foam composite phase change material *Sol. Energy Mater. Sol. Cells* **117** 451–61

[10] Daou I, El-kaddadi L, Zegaoui O, Asbik M and Zari N 2018 Structural , morphological and thermal properties of novel hybrid-microencapsulated phase change materials based on Fe_2O_3 , ZnO and TiO_2 nanoparticles for latent heat thermal energy storage applications *J. Energy Storage* **17** 84–92

[11] Şahan N and Paksoy H 2017 Investigating thermal properties of using nano-tubular ZnO powder in paraffin as phase change material composite for thermal energy storage *Compos. Part B*

[12] Gan L, Lu Z, Cao D and Chen Z 2018 Materials Science & Engineering C E ff ects of cetyltrimethylammonium bromide on the morphology of green synthesized Fe_3O_4 nanoparticles used to remove phosphate *Mater. Sci. Eng. C* **82** 41–5

[13] Aladpoosh R and Montazer M 2015 The role of cellulosic chains of cotton in biosynthesis of ZnO nanorods producing multifunctional properties: Mechanism, characterizations and features *Carbohydr. Polym.* **126** 122–9

[14] Gupta R K, Ghosh K, Dong L and Kahol P K 2010 Green synthesis of hematite (α -Fe_2O_3) submicron particles *Mater. Lett.* **64** 2132–4

[15] Li X, Zhang F, Ma C, Saul E and He N 2012 Green Synthesis of Uniform Magnetite (Fe_3O_4) Nanoparticles and Micron Cubes **12** 2939–42

[16] Kiwumulo H F, Muwonge H, Ibingira C, Lubwama M, Kirabira J B and Ssekitoleko R T 2022 Green synthesis and characterization of iron - oxide nanoparticles using Moringa oleifera : a

potential protocol for use in low and middle income countries *BMC Res. Notes* 1–8

[17] Ramesh A V, Devi D R, Botsa S M and Basavaiah K 2018 Facile green synthesis of Fe_3O_4 nanoparticles using aqueous leaf extract of Zanthoxylum armatum DC . for efficient adsorption of methylene blue *J. Asian Ceram. Soc.* **00** 1–11

[18] Amin M, Kouhbanani J and Beheshtkhoo N 2019 One-step green synthesis and characterization of iron oxide nanoparticles using aqueous leaf extract of Teucrium polium and their catalytic application in dye degradation

[19] Kumar K, Sharma K, Verma S and Upadhyay N 2019 ScienceDirect Experimental Investigation of Graphene-Paraffin Wax Nanocomposites for Thermal Energy Storage *Mater. Today Proc.* **18** 5158–63

[20] Kalantari E, Khalilzadeh M A, Zareyee D and Shokouhimehr M 2020 Catalytic degradation of organic dyes using green synthesized Fe3O4-cellulose-copper nanocomposites *J. Mol. Struct.* **1218**

[21] Wang J, Chen Y, Liu G and Cao Y 2017 Synthesis, characterization and photocatalytic activity of inexpensive and non-toxic Fe_2O_3−Fe_3O_4 nano-composites supported by montmorillonite and modified by graphene *Compos. Part B Eng.* **114** 211–22

[22] Mikhaylov A A, Medvedev A G, Grishanov D A, Sladkevich S, Xu Z J, Sakharov K A, Prikhodchenko P V. and Lev O 2019 Doubly Coated, Organic–Inorganic Paraffin Phase Change Materials: Zinc Oxide Coating of Hermetically Encapsulated Paraffins *Adv. Mater. Interfaces* **6**

[23] Wang J, Xie H, Guo Z, Guan L and Li Y 2014 Improved thermal properties of paraf fi n wax by the addition of TiO 2 nanoparticles **73** 1541–7

[24] Kumar P M, Mylsamy K and Saravanakumar P T 2019 Environmental Effects Experimental investigations on thermal properties of nano-SiO_2 / paraffin phase change material (PCM) for solar thermal energy storage applications *Energy Sources, Part A Recover. Util. Environ. Eff.* **0** 1–14

[25] Nurten Ş, Fois M and Paksoy H 2015 Solar Energy Materials & Solar Cells Improving thermal conductivity phase change materials — A study of paraffin nanomagnetite composites **137** 61–7